Scientific Research Publishing

Materials Sciences and Applications, 2020, 11, 347-369
https://www.scirp.org/journal/msa
ISSN Online: 2153-1188
ISSN Print: 2153-117X

Improvements to Temperature, Warburg Impedance, and Voltage Computations for a Design-Based Predictive Model for Lithium-Ion Capacitors

Davis George Moye[1*], Pedro L. Moss[2], Dhevathi Rajan Rajagopalan Kannan[3], Xujie Chen[#], Omonayo Bolufawi[3], Wanjun Cao[#], Simon Y. Foo[3]

[1]Moye Consultants, Tallahassee, FL, USA
[2]Greencastle Sustainable Electrical Energy Systems, Tallahassee, FL, USA
[3]Department of Electrical and Computer Engineering, Florida A&M University and Florida State University, Tallahassee, FL, USA
Email: *moyeconsultantsreceipts@gmail.com

How to cite this paper: Moye, D.G., Moss, P.L., Kannan, D.R.R., Chen, X.J., Bolufawi, O., Cao, W.J. and Foo, S.Y. (2020) Improvements to Temperature, Warburg Impedance, and Voltage Computations for a Design-Based Predictive Model for Lithium-Ion Capacitors. *Materials Sciences and Applications*, **11**, 347-369.
https://doi.org/10.4236/msa.2020.116024

Received: March 31, 2020
Accepted: May 31, 2020
Published: June 3, 2020

Abstract

An earlier study manipulated the Butler-Volmer equation to effectively model a lithium-ion capacitor's (LIC) energy storage as a function of its constituent components and charge current. However, this model had several shortcomings: computed temperature values were too low, voltage was inaccurate, and the model required Warburg impedance values that were two orders of magnitude higher than experimental results. This study began by analyzing the model's temperature and voltage computations in order to justify output values. Ultimately, these justifications failed. Therefore, in situ temperature rise was measured during charge cycles. Experimental results indicated that temperature increases minimally during a charge cycle (<1%). At high current densities (≥150 $A \cdot kg^{-1}$) temperature increase is negligible. After it was found that LIC temperature change is minimal during a charge cycle, the model accurately computed LIC voltage during the charge cycle and computed Warburg impedance that agreed with values derived from earlier experimental studies, even falling within the measurements' precision error.

Keywords

Lithium-Ion Capacitor, Randles Equivalent Circuit Model, Butler-Volmer Equation

*Corresponding author.
#Freelancers.

1. Introduction

Renewable energy and electrification of the energy sector have surged in popularity as the environmental, economic, and sustainability concerns associated with fossil fuels have called for alternative energy sources. Because renewable energy sources are intermittent and relatively unpredictable, their wholesale integration requires substantial energy storage infrastructure. Additionally, an electric or hybrid electric vehicle requires energy storage. These factors have caused energy storage technology to also see significant attention.

Lithium-ion batteries (LIB) are the most common type of electrochemical energy storage device under development and in use. LIBs are characterized by high specific energy (150 - 200 $W{\cdot}h{\cdot}kg^{-1}$) but low specific power (often below 1 $kW{\cdot}kg^{-1}$) and relatively low cycle lives (2000 cycles for lithium-sulfur, 5000 cycles for lithium titanium dioxide, often lower for other chemistries) [1] [2]. Lithium-ion capacitors (LIC) are a variation of LIB technology that incorporates many aspects of electrochemical double-layer capacitor (EDLC, aka supercapacitor or ultracapacitor) technology. LICs can simultaneously exploit the Faradaic reaction characteristic of a LIB and the non-Faradaic reaction characteristic of an EDLC [3]. Thus LICs are characterized by high specific power (10 $kW{\cdot}kg^{-1}$), long cycle life (e.g. 300,000 cycles in laboratory experiments at General Capacitor) [4] and low specific energy (5 - 10 $Wh{\cdot}kg^{-1}$) [5]. The advantage of LICs is their ability to exploit the high specific energy of LIBs, the high specific power of EDLCs, and the long cycle life of EDLCs.

Often customers seeking energy storage solutions do not base their products on available energy storage technology but have a product under development for which they seek a niche solution. Usually, when a customer considers LIC technology for an application a cell must be prototyped for evaluation, including designing a new form factor and estimating its energy storage, power, and other performance characteristics. There is often trial and error in this process. Building and testing prototypes can be time-consuming, expensive, and therefore a substantial barrier to market entry. Therefore, the LIC industry needs a predictive model that estimates a LIC's performance based upon its design parameters and operating conditions.

Recent research has developed models that can describe both LIB and EDLC voltage and energy storage dynamics as a function of charge or discharge (dis/charge) current and time [6] [7]. But these models describe the performance of an existing energy storage device inside a system as a function of system performance.

Few inroads have been made to dynamically predict LIC energy storage or voltage a function of the electrochemical interactions between the materials that comprise the constituent components of the device. Voltage has been demonstrated as a tool for estimating state of charge in LIBs, while studying their heat generation during dis/charge [8]. And models have been developed to dynamically describe energy storage and dynamic voltage in EDLCs [9]. This EDLC model relies upon the framework of an equivalent circuit model (ECM), like the present study and its antecedent. However, it assumes known impedances and capacitances in the device and does not compute these values from the properties of the constituent components, as the present model does. Because LICs exhibit

Faradaic and non-Faradaic behavior, models predicting LIC behavior from constituent component properties are generally more complex than EDLC models.

Last year Moye *et al.* published the first model to dynamically predict energy storage as a function of the constituent components that comprise a LIC [10]. This model used constituent component properties and dis/charge current to compute the key variables that form a Randles ECM. Then the Randles ECM was able to accurately compute energy storage over a wide range of dis/charge currents. However, this model was limited because it did not accurately compute changes in LIC voltage during a dis/charge cycle. The current study focused upon rectifying this voltage shortcoming and related deficiencies.

The first LIC models simply described experimental results. A common means of doing this is building a Randles ECM to describe a premade, experimental LIC [11] [12]. The Randles ECM attempts to describe an electrochemical device from data on the flow of electricity between its electrolyte and electrodes. This data is usually collected via electrochemical impedance spectroscopy (EIS) and can be interpreted to describe the energy storage device in terms of a series resistance (R_S), a double layer capacitance (C_{dl}), a charge transfer resistance (R_{ct}), and a capacitive element with its own resistance, referred to as the Warburg element (R_W) [13] [14] [15]. A basic Randles ECM topology is shown in **Figure 1**. R_W can be represented in the time domain as shown in **Figure 2** [4] [10].

The earliest LIC modeling studies considered LIC performance as part of a larger system. In 2013 Omar *et al.* [16] developed a LIC model by measuring LIC charge and discharge performance under different temperatures, currents, and states of charge and LIC EIS data at different states of charge. Results were used to build a FreedomCar battery ECM. This study indicated a relationship between current, energy, and temperature. This model and later work by Cao *et al.* only described experimental data and had negligible predictive value.

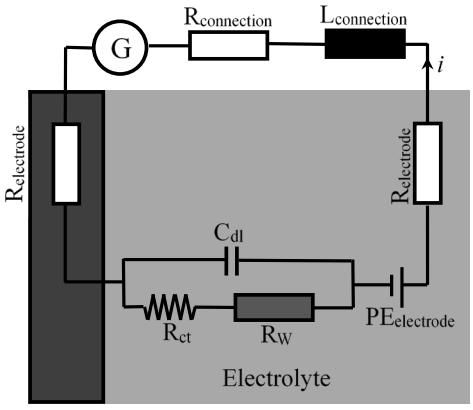

Figure 1. Basic topology of a Randles ECM. G denotes the external circuit. There are three Ohmic resistors, denoted $R_{electrode}$ from the electrodes and $R_{connection}$ from the hardware connecting the energy storage device to the external circuit. These may be combined to a single variable R_s. The loop between G and the energy storage device induces some inductance ($L_{connection}$), although $L_{connection}$ often has a small order of magnitude and is ignored. $PE_{electrode}$ is an assumed ideal voltage source. The movement of electrical charge in the electrolyte is described by R_W, R_{ct}, and C_{dl}.

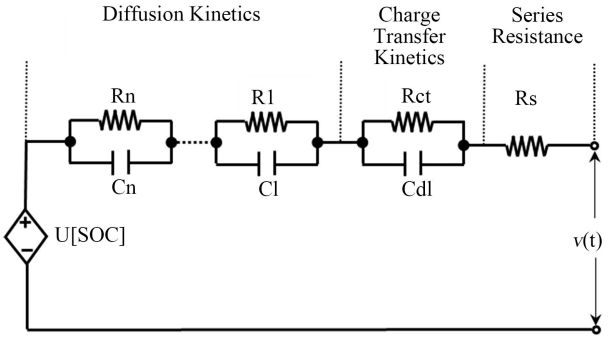

Figure 2. Expanded Randles ECM with a state of charge (SOC) dependency, affecting voltage in the time domain ($v(t)$). This circuit can be represented by a series R_S, a series charge transfer kinetics $R_{ct}C_{dl}$ circuit, and a series Warburg element to describe diffusion kinetics. The Warburg element can be expanded into a series of distinct RC circuits, which are equivalent to R_W in **Figure 1**. Longer chains of RC circuits improve R_W's precision and therefore model fidelity.

The first predictive models involved studies of ambient temperature accelerating cycle life degradation by Uno *et al.* [5] [17]. Uno *et al.*'s work was recently expanded by Moye *et al.* to determine that current has a similar effect on degradation as ambient temperature has [4]. Barcellona *et al.* have developed some predictive LIC models using modified EDLC models [18] [19]. But Barcellona's models rely upon EIS data from finished LICs [20]. These models are useful for predicting a LIC's performance under a certain range of operational conditions. But this range is so limited that Barcellona's models are not ideal for new product design.

Earlier this year Moye *et al.* published a model intended to predict LIC performance as a function of constituent components [10]. This model worked by incorporating relationships determined from earlier experimental studies into a Randles ECM [3] [21]-[27]. Because LICs employ reactions characteristic of both LIBs and EDLCs, modeling research in both of these fields may apply to a LIC model. Of particular concern in LICs is how their internal resistance decreases at high temperatures [21] and that LICs exhibit an inverse relationship between charge and discharge power and energy [23].

1.1. The Previous Version of the Model

This study is preceded by another that developed a model to predict LIC performance as a function of constituent components [15]. The earlier model was the first known physics-based model to predict a LIC's energy storage as a function of its charge current and constituent materials. This initial model was written in Simulink using a Randles ECM framework and relied upon charge current and constituent materials' effects upon the LIC's internal temperature in accordance with the Butler-Volmer equation

$$i_d = i_o\left(\mathrm{e}^{\frac{\alpha_a F_c n_e}{R_u T_q}\eta} - \mathrm{e}^{-\frac{\alpha_c F_c n_e}{R_u T_a}\eta}\right) \tag{1}$$

where i_d is current density, i_o is exchange current density, α_a is the specific surface area of the anode electrode, α_c is the specific surface area of the cathode electrode, n_e is the number of electrons per ion (1 for lithium), η is the activation overpotential, F_c is Faraday's constant, R_u is the universal gas constant, and T_a is the absolute temperature of the electrochemical cell. Because in a LIC the energy storage reaction at the anode is orders of magnitude greater than at the cathode [3], one can assume

$$e^{-\frac{\alpha_c F_c n_e}{R_u T_a}\eta} = 1 \tag{2}$$

Therefore, the Butler-Volmer equation may be rearranged to compute the temperature of the LIC as follows

$$T_a = \frac{\alpha_a n F_c}{R_u \ln\left(\frac{i_d}{i_o - 1}\right)}\eta \tag{3}$$

The Butler-Volmer temperature increase and the LIC's exchange current, in turn, affected the capacitance of the LIC as follows

$$C_W = \frac{c_i R_W^2 F^2 A_s l}{2RT} \tag{4}$$

where C_W is the Warburg capacitance, c_i is the ionic concentration of the electrolyte in moles per kilogram of electrolyte, A_s is the surface area, and l is the thickness of the electrode's active layer [3]. Once these relationships were understood, the model was able to predict energy storage as a function of charge power. Additionally, the model was able to estimate LIC voltage and therefore state of charge.

This model computed energy storage within 4% accuracy over a wide range of charge powers, as shown in **Figure 3**.

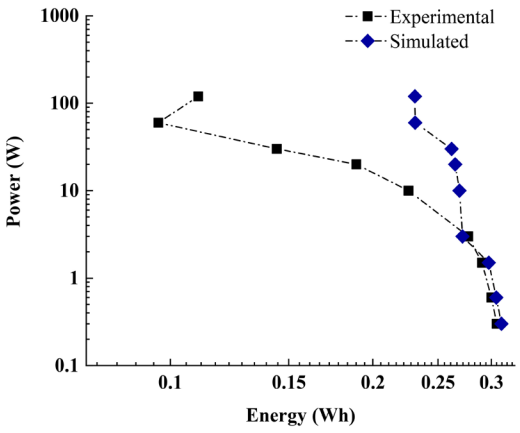

Figure 3. Chart comparing experimental and modeled LIC energy storage over a wide range of charge powers, ranging from 0.3 - 120 A. Notice that for a LIC energy storage varies as much as 300%. Also notice that energy storage increases slightly at very higher power [10].

Of note, energy storage may range as much as 300%, depending upon charge power, but performance is not linear. For example, energy storage increases slightly at very high power (≈120 W or 6 kW·kg^{-1}). Other studies indicate electrolyte breaks down at high temperature [28]. Electrolyte breakdown momentarily adds additional ions to the solution that have the effect of increasing energy storage [4] [10]. Because

$$i_d = \frac{i}{A} \tag{5}$$

where i is current and A is the surface area, Equation (3) implies

$$i \propto \frac{1}{T_a} \tag{6}$$

Many efforts have been applied to model known energy storage devices as a function of temperature and other variables (e.g. [16] [29]), but this is the study and its predecessor are the first attempts to predict a LIC's performance as a function of its constituent components. Another potential concern is hysteresis, as temperature effects on a device may not be observed immediately [30]. A cornerstone of this study is Uno and Tanaka's previous work demonstrating that elevated temperature in LICs degrades them in a similar manner as elevated current does [5]. This relationship and its implications are a cornerstone of this study.

1.2. Deficiencies in the Previous Version of the Model

Voltage in the model should be computed as a sum of all voltage drops across major RC elements in the Randles ECM depicted in **Figure 2**. Voltage drops across all series (V_S), double layer ($V_{dl//CT}$), and Warburg (V_W) elements are given by Equations (7)-(9), respectively.

$$V_S = iR_S \tag{7}$$

$$V_{dl} = iR_{ct}\left(1 - \mathrm{e}^{-\frac{t}{R_{ct}C_{dl}}}\right) \tag{8}$$

$$V_W = iR_W\left(1 - \mathrm{e}^{-\frac{t}{R_W C_W}}\right) \tag{9}$$

And Equation (9) is rewritten for every branch, n, of the equivalent R_W elements as follows

$$V_n = iR_n\left(1 - \mathrm{e}^{-\frac{t}{R_n C_n}}\right) \tag{10}$$

So that

$$V_W = V_1 + V_2 + \cdots + V_n \tag{11}$$

The total voltage increase, V_T, can be expressed by

$$V_T = V_s + V_{dl} + V_W \tag{12}$$

This model could not accurately compute the voltage. Error was low at very high charge power but averaged 30% at low charge power. This is important because voltage is often used to indicate the state of charge in a capacitor.

Reinvestigation identified some discrepancies in temperature computations. The temperature was computed from the model's computed capacitance (T_{mod}) and from experimental energy storage (T_{exp}), using Equation (4) and a modification of the relationship between capacitance and energy

$$E = \frac{1}{2} C \Delta V^2 \tag{13}$$

where E is energy stored, C is capacitance, and ΔV is the change in voltage. In this situation C will be replaced by C_T, a total capacitance variable, which includes both C_W and a non-temperature dependent double-layer capacitance (C_{dl}) as follows

$$C_T = C_W + C_{dl} \tag{14}$$

C_{dl} is found by

$$C_{dl} = \frac{F_c \rho l}{2M} (1 - \varepsilon) \frac{l}{l_s} \tag{15}$$

where ρ is the density of the electrode material, M is the mass of the active material, ε is the porosity of the electrode material, l is the thickness of the electrode, and l_s is the thickness of the separator material between the electrodes.

These results showed moderate agreement between T_{mod} and T_{exp}, except at high power, as shown in Figure 4. However, all tests were performed in a room with an ambient temperature of 300 K. Thus the low power experimental temperature values and all model temperature computations, which hovered near 150 K, were suspect and called for a reassessment of the model's computations.

In order to understand how T_a impacts V, a fit equation was computed from T_{exp} in order to determine T as a function of P as follows

$$T = -0.0006P^3 + 0.0617P^2 + 3.1543P + 131.0 \tag{16}$$

Use of this equation improved V calculations as shown in Figure 5. Of note, improvements in the accuracy of T_a improve the model's computation of V. However, improving T_a does not eliminate all error, especially at low power.

1.3. Abbreviations and Acronyms

This data indicated that error in T computations only partially addressed the error in V. Equation (2), used to compute T_a, computes T_a as a function of η, i_d, and i_o, but is unaffected by R_W. By contrast, T_{exp} relies upon Equation (3), which considers R_W. Subsequent experiments reverted to computing T_a using Equation (2) and studied R_W's effects upon the circuit because R_W had previously received little attention. Upon examination it was hypothesized that because R_W is divided into four smaller RC circuits, each of which has its own impact on temperature (Figure 2), T_{exp} may have been misinterpreted as a temperature change

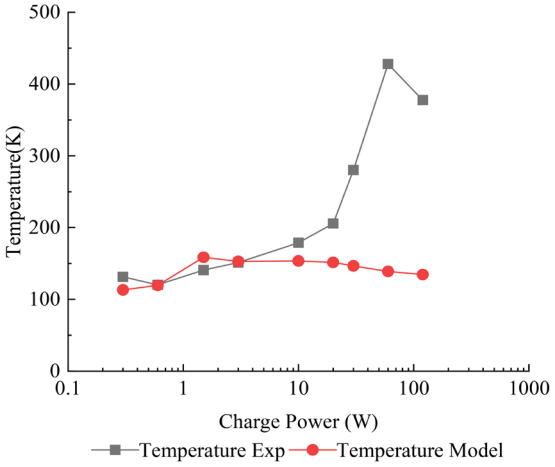

Figure 4. T_a computed from energy storage, comparing T_a computed from experimental energy storage computations and T_a computed from the model's energy storage computations. Notice that both T_a computations are much colder than the room temperature (300 K), and their precision diverges above 10 W. These values indicate that although the model output an accurate energy storage value, some of its underlying computations were not accurate.

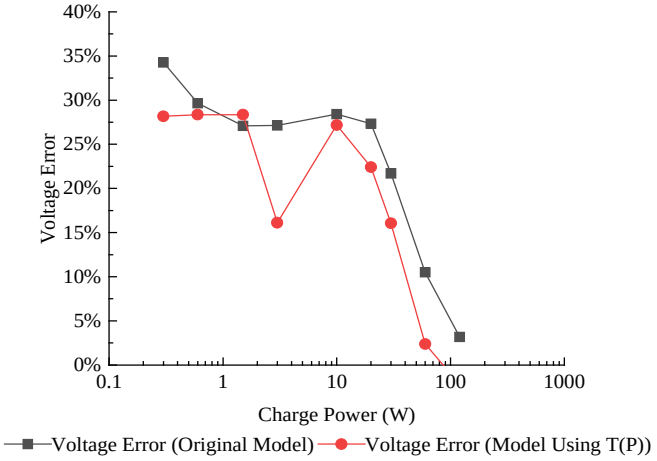

Figure 5. Comparison of percent error in the original model and original model modified to compute temperature as a function of power. This comparison was made in order to determine if the model had a calibration problem or if the underlying computations were inaccurate. The lack of precision in voltage error indicates an underlying computation was incorrect.

across each of the *RC* circuits, implying

$$T_{mod} = 4 \times T_{exp} \tag{17}$$

In order for this to be accurate, R_W had to be adjusted to change with charge current. If changes in the model's R_W input led to matches in experimental and modeled E and V, and if Equation (17) is correct, then the R_W value may be computed as the only missing variable. Under this assumption R_W showed a predictable relationship with respect to charge power, but this relationship broke down around 30 W, spiking at 60 W, as shown in **Figure 6**.

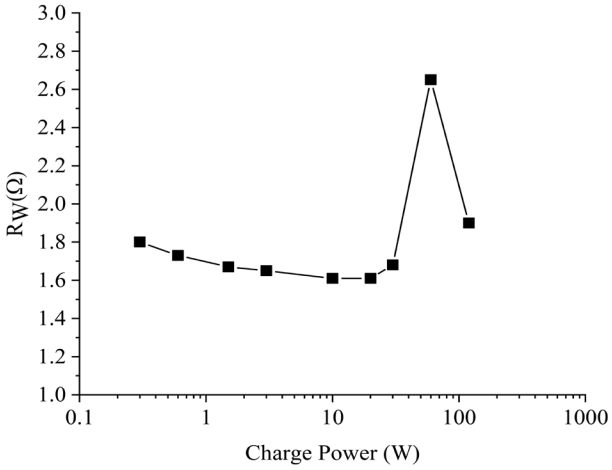

Figure 6. Optimal R_W values calculated as a function of charge power. In order for the first version of the model to be accurate, R_W must reflect these values. These values are two orders of magnitude higher than those reflected in the previous study's EIS experiments and were eventually determined to be a major source of the error shown in **Figure 4** and **Figure 5**.

This relationship can be approximated as

$$R_W = -8\times10^{-6}P^3 + 0.0013P^2 - 0.0103P + 1.7604 \tag{18}$$

The reason for this spike in R_W at 60 W is probably the same as the culprit for C_T's increases at very high power. This phenomenon of increasing C_T is probably due to electrolyte breaking down at high temperature and increasing the number of ions that could carry charge inside the LIC [10] [28]. An increase in C_T can be mathematically accommodated by an increase in R_W in accordance with Equations (3) and (12). Earlier studies indicate R_W increases with temperature, but these studies employed low charge currents (0.2 mA/cm^2) and studied relatively low ambient temperatures (−20˚C - +70˚C) [31], so they may have not incorporated many of the capacitive aspects of a LIC. By contrast, at 30 W the charge current is approximately 360 mA/cm^2 and the T variable has increased by 30% over its values below 10 W. Experimentalists do not yet understand these high power dynamics. Below 30 W charge power, R_W can be approximated as

$$R_W = -4\times10^{-5}P^3 - 0.0012P^2 - 0.0222P + 1.7195 \tag{19}$$

These R_W values identified in **Figure 6** and explained in Equation (18) and Equation (19) all rendered less than 1% error in voltage. They also yielded good agreement between experimentally-computed temperature (T_{exp}) and temperature computed from the model's $C_W(T_{check})$. However, as shown in **Figure 7**, T_{exp} and T_{check} did not agree with T in accordance with Equation (17).

In order to verify T_a's accuracy, temperature increase was computed across each of the four R_WC_W elements in series (R_1C_1, R_2C_2, R_3C_3, R_4C_4) using Equation (17) and $R_{ct}C_{dl}$ using a modified Equation (2), as follows

$$T_a = \frac{R_{CT}nFi_o}{R_u} \tag{20}$$

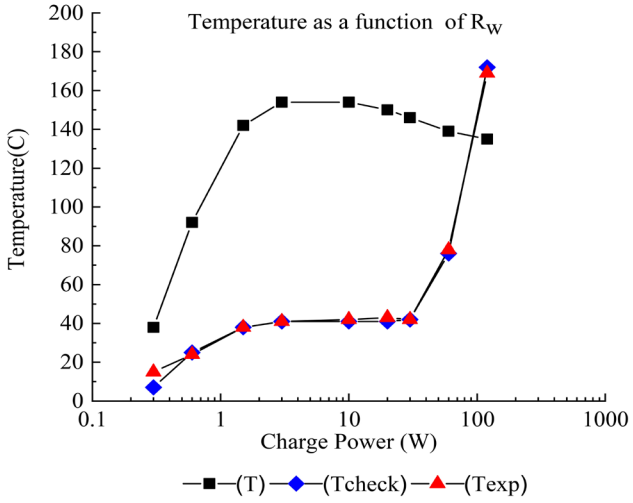

Figure 7. Temperature initially computed by the model (T_{mod}), computed by the model in order to verify C_w (T_{check}), and experimentally (T_{exp}). Notice T does not equal 4 × T_{exp} or 4 × T_{check}. In order for the R_W values shown in **Figure 6** to be accurate T_{check} and T_{exp} must agree with T. Because they do not, serious doubt is cast upon the R_W values used.

This temperature increase was designated T_{check2}. T_{check2} and T_{check} must obey Equation (17) in order to be valid. $R_{ct}C_{dl}$'s contribution to T_a is negligible at all charge powers. For example, at 60 W, where the temperature was computed to be highest,

$$T_{R_{CT}/\!/C_{dl}} = \frac{0.09\times 1\times 96485\times 7.6\times 10^{-8}}{8.314} = 7.9\times 10^{-5} \tag{21}$$

Consequently, the following approximation is valid for T_{check2}

$$T_{check\,2} = \frac{c_i R_1^2 F^2 A_s l}{2RC_1} + \frac{c_i R_2^2 F^2 A_s l}{2RC_2} + \frac{c_i R_3^2 F^2 A_s l}{2RC_3} + \frac{c_i R_4^2 F^2 A_s l}{2RC_4} \tag{22}$$

T_{mod}, T_{check}, T_{exp}, and T_{check2} are compared in **Figure 8**.

T_{check2} is four times T_{check} at all charge powers, satisfying Equation (17). Also, T_{check2} agrees well with T at all powers until P is 30 W, after which error increases, maximizing at 60 W, where R_W spikes. At 60 W and 120 W T_{check2} continues to be four times as large as T_{exp} and T_{check}. But T decreases to within 50% of T_{exp} and T_{check}. Consequently, Equation (17) is only reliably satisfied below 30 W, where T is reliable. Further research into electrolyte breakdown at high temperatures and/or current is needed to provide more insight into this phenomenon and to enable effective modeling.

Using the methods described above, computing T from Equation (2), and computing R_W from Equations (18) or (19), error in V's final value was less than 1%, and error in E remains negligible. Although the model gave accurate results regarding energy storage and voltage, it still had two serious deficiencies:

- There was no in-situ data to validate the computation of T. All T values had been theoretically computed from the Butler-Volmer equation and various derivations, Equations (1)-(3), (13), and (20). Some direct, experimental temperature data was needed in order to assess this.

- In order for the model to work properly, R_W had to be on the order of 1.5 Ω, as shown in Figure 6. But experimental EIS data from the previous study indicated R_W should be on the order of 0.015 Ω.

2. Experimental Work

2.1. Temperature Change Study

As in the previous study [10], a 200F LIC made by General Capacitor (product number LCA200G1, shown in Figure 9, was used to provide experimental data as a baseline to compare against the model. The reasons for this choice are twofold.

- At the time General Capacitor's 200F product was widely marketed and was commercially available.
- The previous version of the model computed a theoretical temperature increase for LCA200G1, which needed to be validated or disproven.

LCA200G1 design specifications are shown in Table 1. All experimental data in this study came from a LCA200G1 made using the method described by Cao *et al.* [27]. Because LCA200G1 was a commercial, flagship product, much data had already been collected about its performance, including cycle life data, which can take months, if not years to collect. Additionally, many components and operational parameters, including separator material, electrolyte, operating voltage range, and current collector tab position and welding methods were well-known and likely to be repeated by General Capacitor. This eliminated much of the variability often encountered in laboratory-made LICs.

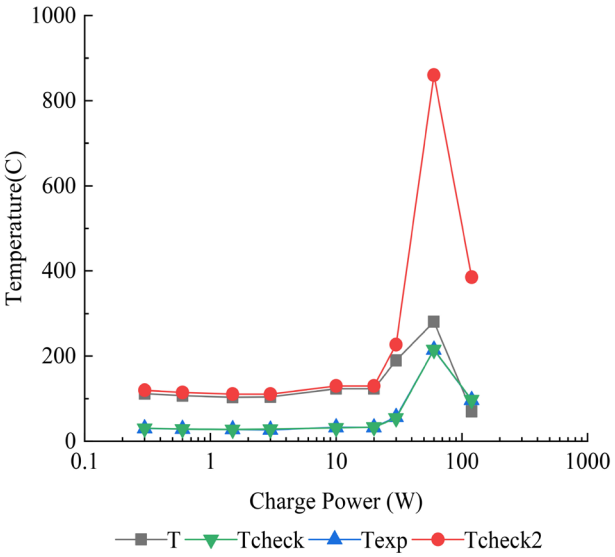

Figure 8. Temperature initially computed by the model (T), computed by a combination of all four RC circuits comprising the Warburg elements (T_{check2}), computed by the model in order to verify C_w (T_{check}), and experimentally (T_{exp}). The agreement between T_{check2}, T_{check} (using Equation (17)). T_{exp} (using Equation (17)), and T indicate the model may have initially computed properly, only requiring calibration. Of note, there were not yet any in situ data temperature measurements to validate these computations.

Figure 9. LCA200G1, the flagship 200F LIC product made by General Capacitor.

Table 1. Specifications of General Capacitor LCA200G1, flagship nominal 200F product made by General Capacitor.

Parameter	Value
Lithium Source	Foil Strips
Positive Electrode Active Material	Activated Carbon
Positive Electrode Active Layer Thickness	100 μm
Double-Sided Positive Electrodes	7
Negative Electrode Active Material	Hard Carbon
Negative Electrode Active Layer Thickness	90 - 95 μm
Double-Sided Negative Electrodes	6
Single-Sided Negative Electrodes	2
Negative Electrode Lithium Loading	8.81%
Negative Electrode Porosity	44.16%
Positive Electrode : Negative Electrode Mass Ratio	0.678
Lithium Source	Foil Strips
Positive Electrode Active Material	Activated Carbon
Positive Electrode Active Layer Thickness	100 μm
Double-Sided Positive Electrodes	7

As discussed in section 1.3, the experimental validation of the theoretical T value was required in order to validate model's accuracy. Because the test LICs were handled shortly after testing, it was doubtful that the actual ΔT was any higher than a few Kelvin. The initial hypothesis was that the actual ΔT was only slightly lower than the experimental value because of thermal insulating effects inside the LIC. Results indicated the temperature question is more complex than this, as will be explained. Results are shown in Figure 10. At high power charges no temperature increase was observed, as shown by the 10 W charge in Figure 9 and as anticipated by Equation (6). The ΔT values observed at all of these charge powers are compared in Figure 11.

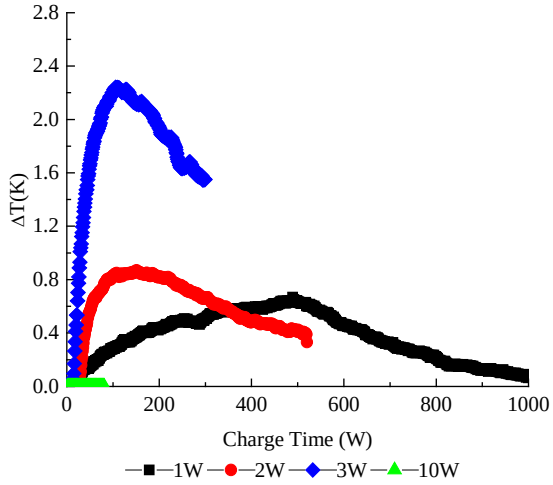

Figure 10. Comparison of ΔT rise with time at constant power charge. Notice ΔT peaks then lowers. This is probably a factor of current adjusting for voltage. Notice ΔT equals 0 for the 10W charge.

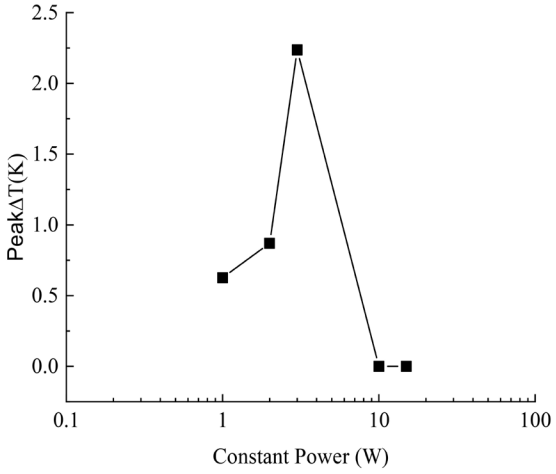

Figure 11. Comparison of total ΔT increase as a function of power charge. Notice a strong correlation between peak ΔT and charge power until 3 W, nominally 1 A. This correlation breaks down at higher power.

In Figure 9 ΔT peaks then decrease again. This is probably a byproduct of current changes due to Ohm's law. Because of voltage changes during a charge, a constant power charge will begin with a high current when the voltage is low and end with a low current when the voltage is high. Therefore, near the end of a charge, there is less current to affect the temperature of the LIC. In order to more directly assess the effects of current upon temperature, constant current measurements were made. At currents below 1.0 A, these results showed a linear temperature increase with time. At a higher current, 5.0 A, no temperature increase was measured. 5.0 A was the limit of test equipment. These results are shown in Figure 12. They indicate the Butler-Volmer equation's temperature increase appears to accurately link current and temperature at relatively low current, but this relationship breaks down at higher currents, where more capacitive behavior dominates. There appears to be a hysteresis as charge current does not immediately affect temperature. Above a certain threshold the charge cycle finishes before current's effects on cell temperature can be felt. The reason for this is not understood.

If the 5.0 A charging data is ignored, the slope of the charge temperature increases linearly with charge current and can be predicted by an equation

$$\Delta T_{Slope} = 0.0043i \tag{23}$$

which is plotted in Figure 13. In terms of current density, this is

$$\Delta T_{Slope} = 1\times 10^{-5} i_d \tag{24}$$

as demonstrated in Figure 14.

The results shown in Figures 9-14 indicated what the value of ΔT used in the model should be. These experimental ΔT values were used to calibrate the model. First, the initial ambient temperature was set at 298 K, the nominal ambient temperature of the environmental test chamber where the study was conducted. As the maximum ΔT was 2.24 K, the change in the T variable is less than 1% when operating at room temperature. Thus T may be treated as a constant in many circumstances.

2.2. R_W Improvements

As discussed earlier, another problem with the previous model is that R_W was considered static. In fact, it is not. The values found in Figure 6 and Equations (16) and (17) were two orders of magnitude higher than the experimental value of 0.011 Ω computed from potentiostatic EIS data, using a maximum current of 0.1 A. In order to improve the model, another approach was adopted, found by Greenleaf *et al.* in an earlier study [32]. This approach computes R_W as follows

$$R_W = \frac{R_u T \delta}{n^2 F^2 C_s^2 A\sqrt{2} D_s} \tag{25}$$

where D_s is the species' diffusion coefficient, δ is the Nernst diffusion coefficient, found from the effective particle radius (r) of the negative electrode material as follows

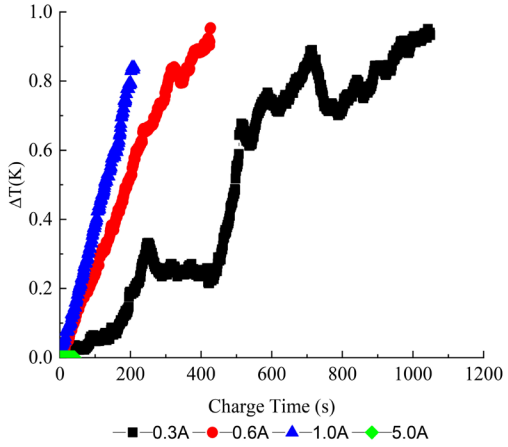

Figure 12. Comparison of ΔT rise with time at constant current. Notice all curves are nearly linear. At lower charge currents observe more perturbations in the slope of ΔT. There appears to be a hysteresis as charge current's effects are not immediately felt on ΔT. Moreover, their effects are not consistently felt at low current (0.3 A and to a lesser extent 0.6 A). However, at high current (5.0 A) ΔT equals 0. This may have been because the cell had finished charging before current's effects on temperature had been felt.

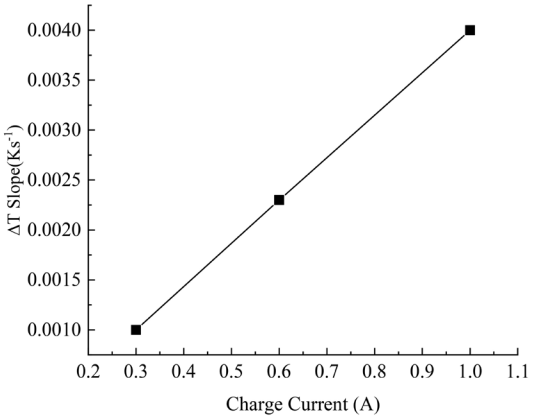

Figure 13. ΔT_{slope} with charge current. Notice this linear relationship only holds valid at low current. Not shown in this chart, ΔT's slope was 0 at 5.0 A.

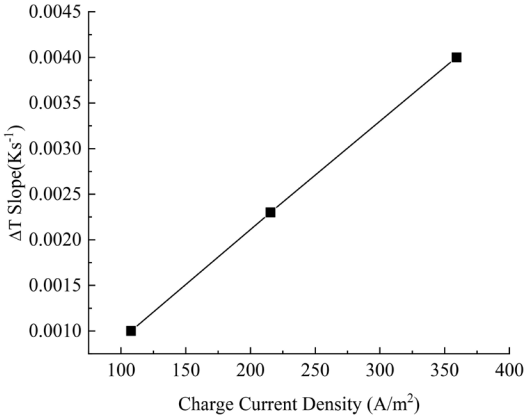

Figure 14. ΔT_{slope} with charge current density at low current density. Higher current densities, where this relationship breaks down are not shown.

$$\delta = \frac{r}{5} \tag{26}$$

r for the hard carbon material in this anode is approximately 50 μm, making δ equal to 10 μm.

R_W values calculated using Equation (20) and experimental ΔT data agreed with experimental values found from the previous study's EIS data that were used to build the previous study's model. This data anticipates R_W values on an order of magnitude similar to the EIS data. Results are compared in Figure 15.

This R_W computation method was combined with the revised method of calculating ΔT. Once R_W was computed by Equation (20) and used accurate ΔT values, error in V diminished but was not eliminated. When the lowest computed R_W value was used, 0.013 Ω, error in the final V value was less than 5%. R_W and energy computations matched experimental values. Energy computations never appreciably changed. The voltage drop across R_S is very small, 5.4 mV, so it does not appreciably affect ΔV. These results also indicate that R_W should be treated as a constant and does not change with current. Voltage error is compared in Figure 16.

One limitation of this method, however, is that the model initially increases V very quickly with high error, although V eventually levels off, as shown in Figure 17. Upon examination of V_S, $V_{dl//CT}$, V_W, it is found $V_{dl//CT}$ is the primary source of this error, as it increases by 1 V during the first several seconds of a charge but is then constant. More research is needed to determine why $V_{dl//CT}$ behaves in this manner and to correct it. Because the problem has been isolated to $V_{dl//CT}$, it is believed the model may struggle with the non-Faradaic, capacitor behavior in an LIC more so than the Faradaic, battery behavior.

2.3. Model Adjustments from Temperature Change

The only other unknown left in Equation (2) was η. η values that agreed with experimental results shown in Figures 9-11 were found and are shown in Figure 18. The method of computing R_W had minimal impact on η. Because T is relatively constant these results caused η to decrease by two orders of magnitude when compared to the previous model.

3. Conclusions

The previous study's model was improved with experimental data and additional theoretical relationships. The first step was to compute temperature values from the model's predicted energy storage and from experimentally measured energy storage. This method used energy storage's implications on Warburg capacitance and Warburg capacitance's implications on cell temperature. These temperature values were analyzed, but they gave values that were lower than expected. Experimental measurements were taken and used to validate the temperature variables. The experimental results indicated that although the temperature does increase as an LIC is charged, this increase is small, <1%. However,

the model could only explain these results at relatively low current, where battery behavior dominates. Where capacitive behavior is more pronounced, the model breaks down and indicates negligible temperature increases. In order for the model to accurately reflect the experimental temperature values, the overpotential variable needed to be significantly reduced from the previous study. In fact, the temperature increases are so small that the overpotential variable has little impact on the overall model. The model was adjusted to compute Warburg impedance, which then agreed with the EIS values published in the previous study. It was discovered that Warburg impedance behaves as a constant variable. The result is an improved Butler-Volmer based model that computes energy storage as a function of charge power, also accurately computing voltage and temperature.

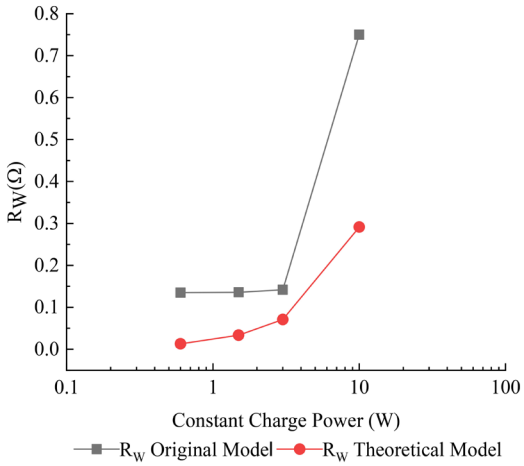

Figure 15. Comparison of R_W values used in the first iteration (R_W Original Model) and R_W computed by equation (R_W Theoretical Model).

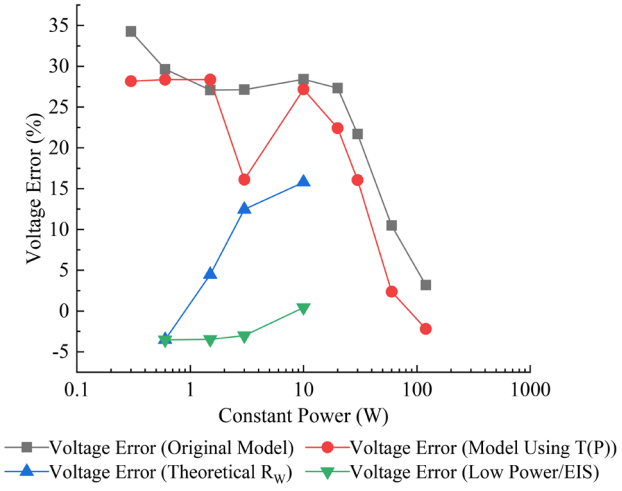

Figure 16. Comparison of per cent error in voltage from the original model, model computing temperature as a function of power, and from several data points, where the model temperature matched the check temperature. Notice voltage error is very low when the model's temperature matched its checking mechanism.

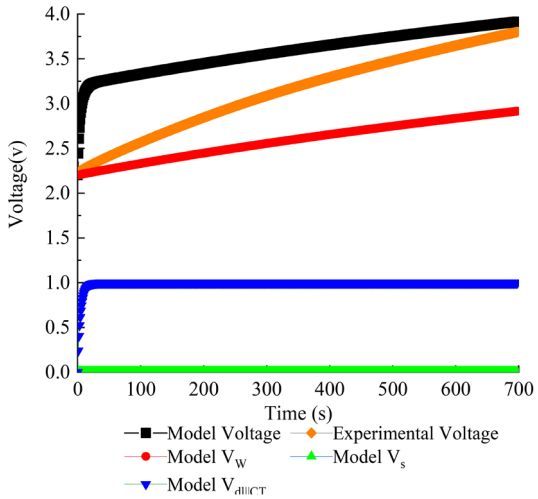

Figure 17. Comparison of voltage computed by model, voltage computed by experiment, and the contributions of. V_S, $V_{dl//CT}$, and V_W. Notice that initially, the model spikes voltage, but there is a close agreement at the end of the charge. These voltage computations enable researchers to understand voltage drops, and therefore power and therefore energy stored via Faradaic, LIB mechanisms, non-Faradaic, EDLC mechanisms, and simple Ohmic losses. Thus the model explains the extent to which the theoretical LIC behaves like a battery, a capacitor, or a resistor.

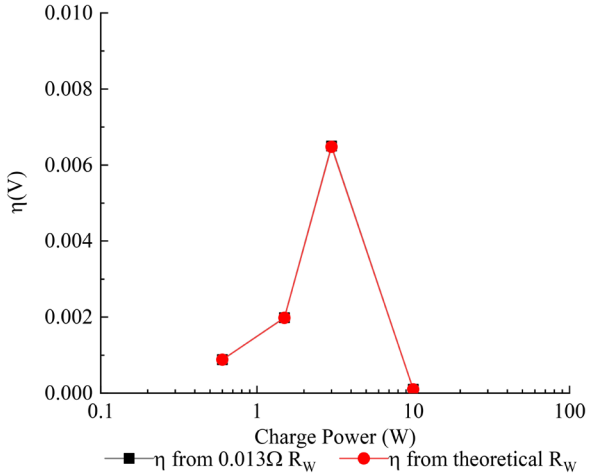

Figure 18. Changes to η values after new values had been found for ΔT and R_W. Notice agreement is very high, indicating the model properly computes η.

There are several shortcomings to model as it now stands. Additional experimental data would be useful to improve the calibration of the model's temperature variables. However, it is unlikely that additional experimental data would cause a significant improvement in voltage and energy storage modeling below 10 W or 3.3 A. Above 10 W the model's voltage value initially overshoots experimental data, resulting in voltage error that is initially very high. But the model's voltage becomes accurate near the end of the charge cycle. This initial overshoot appears to be caused by the model's treatment of the non-Faradaic, capacitor behavior in the LIC and merits further investigation.

Specific findings from this study were:

- Improved understanding of temperature changes during LIC charging. Specifically, LIC temperature increases little during a charge cycle. This increase is linear vs. time and charge current. However, above a certain threshold current, temperature rise is negligible. In all cases temperature rise is >1%. Future studies may approximate temperature as a constant.
- Mathematical verification that R_W values in LIC models are on the order of 0.01 - 0.02 Ω.
- An improved model that computes LIC energy storage and voltage as a function of the LIC's constituent components, ambient temperature, and charge current.

Acknowledgements

This research was performed using the resources of General Capacitor LLC and Moye Consultants LLC.

Conflicts of Interest

The authors declare no conflicts of interest regarding the publication of this paper.

References

[1] Yao, S., Tang, H., Liu, M., Chen, L., Jing, M., Shen, X., Li, T. and Tan, J. (2019) TiO_2 Nanoparticles Incorporation in Carbon Nanofiber as a Multi-Functional Interlayer toward Ultralong Cycle-Life Lithium-Sulfur Batteries. *Journal of Alloys and Compounds*, **788**, 639-648. https://doi.org/10.1016/j.jallcom.2019.02.236

[2] Shi, Y., Yang, D., Yu, R., Liu, Y., Hao, S.M., Zhang, S., Qu, J. and Yu, Z.Z. (2018) Robust Binder-Free Anodes Assembled with Ultralong Mischcrystal TiO_2 Nanowires and Reduced Graphene Oxide for High-Rate and Long Cycle Life Lithium-Ion Storage. *Journal of Power Sources*, **383**, 115-123. https://doi.org/10.1016/j.jpowsour.2018.02.046

[3] Zheng, J. (2003) The Limitations of Energy Density of Battery/Double-Layer Capacitor Asymmetric Cells. *Journal of the Electrochemical Society*, **150**, A484-A492. https://doi.org/10.1149/1.1559067

[4] Moye, D.G. (2019) A Predictive Model of Design Performance for Lithium-Ion Capacitors. PhD Dissertation, Florida State University, Tallahassee.

[5] Uno, M. and Tanaka, K. (2012) Accelerated Charge-Discharge Cycling Test and Cycle Life Prediction Model for Supercapacitors in Alternative Battery Applications. *IEEE Transactions on Industrial Electronics*, **59**, 4704-4712. https://doi.org/10.1109/TIE.2011.2182018

[6] Wang, Y., Liu, C., Pan, R. and Chen, Z. (2017) Modeling and State-of-Charge Prediction of Lithium-Ion Battery and Ultracapacitor Hybrids with a Co-Estimator. *Energy*, **121**, 739-750. https://doi.org/10.1016/j.energy.2017.01.044

[7] Wang, Y., Gao, G., Li, X. and Chen, Z. (2020) A Fractional-Order Model-Based State Estimation Approach for Lithium-Ion Battery and Ultra-Capacitor Hybrid Power Source System Considering Load Trajectory. *Journal of Power Sources*, **449**, Article ID: 227543. https://doi.org/10.1016/j.jpowsour.2019.227543

[8] Srinivasan, V. and Wang, C.Y. (2003) Analysis of Electrochemical and Thermal Behavior of Li-Ion Cells. *Journal of the Electrochemical Society*, **150**, A98-A106. https://doi.org/10.1149/1.1526512

[9] Quintana, J.J., Ramos, A. and Nuez, I. (2013) Modeling of an EDLC with Fractional Transfer Functions Using Mittag-Leffler Equations. *Mathematical Problems in Engineering*, *Special Issue*: *Advanced Topics in Dynamics of Complex Systems*, **2013**, Article ID: 807034. https://doi.org/10.1155/2013/807034

[10] Moye, D.G., Moss, P.L., Chen, X., Cao, W.J. and Foo, S.Y. (2019) A Design-Based Predictive Model for Lithium-Ion Capacitors. *Journal of Power Sources*, **433**, Article ID: 226694. https://doi.org/10.1016/j.jpowsour.2019.226694

[11] Cao, W. and Zheng, J. (2013) The Effect of Cathode and Anode Potentials on the Cycling Performance of Li-Ion Capacitors. *Journal of the Electrochemical Society*, **160**, A1572-A1576. https://doi.org/10.1149/2.114309jes

[12] Cao, W., Greenleaf, M., Li, Y., Adams, D., Hagen, M., Doung, T., *et al.* (2015) The Effect of Lithium Loadings on Anode to the Voltage Drop during Charge and Discharge of Li-Ion Capacitors. *Journal of Power Sources*, **280**, 600-605. https://doi.org/10.1016/j.jpowsour.2015.01.102

[13] Randles, J.E.B. (1947) Kinetics of Rapid Electrode Reactions. *Discussions of the Faraday Society*, **1**, 11-19. https://doi.org/10.1039/df9470100011

[14] Hampson, N., Karunathilaka, S. and Leek, R. (1980) The Impedance of Electrical Storage Cells. *Journal of Applied Electrochemistry*, **10**, 3-11. https://doi.org/10.1007/BF00937331

[15] Moss, P.L., Zheng, J.P., Ao, G., Cygan, P.J. and Plichta, E.J. (2007) Transmission Line Model for Describing Power Performance of Electrochemical Capacitors. *Journal of the Electrochemical Society*, **154**, A1020-1025. https://doi.org/10.1149/1.2778126

[16] Omar, N., Ronsmans, J., Firozu, Y., Monem, M.A., Samba, A., Gualous, H., *et al.* (2013) Lithium-Ion Capacitor—Advanced Technology for Rechargeable Energy Storage Systems. *Electric Vehicle Symposium and Exhibition* (*EV*S27), Barcelona, 17-20 November 2013, 1-11. https://doi.org/10.1109/EVS.2013.6914718

[17] Uno, M. and Kukita, A. (2016) Cycle Life Evaluation Based on Accelerated Aging Testing for Lithium-Ion Capacitors as Alternative to Rechargeable Batteries. *IEEE Transactions on Industrial Electronics*, **63**, 1607-1617. https://doi.org/10.1109/TIE.2015.2504578

[18] Barcellona, S., Ciccarelli, F., Iannuzzi, D. and Piegari, L. (2014) Modeling and Parameter Identification of Lithium-Ion Capacitor Modules. *IEEE Transactions on Sustainable Energy*, **5**, 785-794. https://doi.org/10.1109/TSTE.2014.2301950

[19] Musolino, V., Piegari, L. and Tironi, E. (2013) New Full-Frequency-Range Supercapacitor Model with Easy Identification Procedure. *IEEE Transactions on Industrial Electronics*, **60**, 112-120. https://doi.org/10.1109/TIE.2012.2187412

[20] Barcellona, S. and Piegari, L. (2017) A Lithium-Ion Capacitor Model Working on a Wide Temperature Range. *Journal of Power Sources*, **342**, 241-251. https://doi.org/10.1016/j.jpowsour.2016.12.055

[21] Cao, W., Li, Y., Fitch, B., Shih, J., Doung, T. and Zheng, J. (2014) Strategies to Optimize Lithium-Ion Supercapacitors Achieving High-Performance: Cathode Configurations, Lithium Loadings on Anode, and Types of Separator. *Journal of Power Sources*, **268**, 841-847. https://doi.org/10.1016/j.jpowsour.2014.06.090

[22] Cao, W. and Zheng, J. (2012) Li-Ion Capacitors with Carbon Cathode and Hard

Carbon/Stabilized Lithium Metal Powder Anode Electrodes. *Journal of Power Sources*, **213**, 180-185. https://doi.org/10.1016/j.jpowsour.2012.04.033

[23] Cao, W.J., Shih, J., Zheng, J.P. and Doung, T. (2014) Development and Characterization of Li-Ion Capacitor Pouch Cells. *Journal of Power Sources*, **257**, 388-393. https://doi.org/10.1016/j.jpowsour.2014.01.087

[24] Sikha, G., Popov, B.N. and White, R.E. (2004) Effect of Porosity on the Capacity Fade of a Lithium-Ion Battery Theory. *Journal of the Electrochemical Society*, **151**, A1104-A1114. https://doi.org/10.1149/1.1759972

[25] Sikha, G., White, R.E. and Popov, B.N. (2005) A Mathematical Model for a Lithium-Ion Battery/Electrochemical Capacitor Hybrid System. *Journal of the Electrochemical Society*, **152**, A1682-A1693. https://doi.org/10.1149/1.1940749

[26] Cao, W., Zheng, J., Adams, D., Doung, T. and Zheng, J.P. (2014) Comparative Study of the Power and Cycling Performance for Advanced Lithium-Ion Capacitors with Various Carbon. *Journal of the Electrochemical Society*, **161**, A2087-A2092. https://doi.org/10.1149/2.0431414jes

[27] Cao, W., Luo, J., Yan, J., Chen, X., Brandt, W., Warfield, M., *et al.* (2017) High Performance Li-Ion Capacitor Laminate Cells Based on Hard Carbon/Lithium Stripes Negative Electrodes. *Journal of the Electrochemical Society*, **164**, A93-A98. https://doi.org/10.1149/2.0351702jes

[28] Boltersdorf, J., Delp, S.A., Yan, J., Cao, B., Zheng, J.P., Jow, T.R., *et al.* (2018) Electrochemical Performance of Lithium-Ion Capacitors Evaluated under High Temperature and High Voltage Stress Using Redox Stable Electrolytes and Additives. *Journal of Power Sources*, **373**, 20-30. https://doi.org/10.1016/j.jpowsour.2017.10.084

[29] Tang, X., Wang, Y., Zou, C., Yao, K., Xia, Y. and Gao, F. (2019) A Novel Framework for Lithium-Ion Battery Modeling Considering Uncertainties of Temperature and Aging. *Energy Conversion and Management*, **180**, 162-170. https://doi.org/10.1016/j.enconman.2018.10.082

[30] Wang, Y. and Chen, Z. (2020) A Framework for State-of-Charge and Remaining Discharge Time Prediction Using Unscented Particle Filter. *Applied Energy*, **260**, Article ID: 114324. https://doi.org/10.1016/j.apenergy.2019.114324

[31] Yoshino, A., Tsubata, T., Shimoyamada, M., Satake, H., Okano, Y., Mori, S. and Yata, S. (2004) Development of a Lithium-Type Advanced Energy Storage Device. *Journal of the Electrochemical Society*, **15**, A2180-A2182. https://doi.org/10.1149/1.1813671

[32] Greenleaf, M., Li, H. and Zheng, J.P. (2014) Application of Physical Electric Circuit Modeling to Characterize Li-Ion Battery Electrochemical Processes. *Journal of Power Sources*, **270**, 113-120. https://doi.org/10.1016/j.jpowsour.2014.07.083

Appendix

Nomenclature	
A	Ampere
A_s	surface area
C	capacitor
C_{dl}	double layer capacitance
c_i	ionic concentration of electrolyte
C_T	total capacitance
C_W	Warburg capacitance
D_S	diffusion coefficient
E	energy
ECM	equivalent circuit model
EDLC	electrochemical double layer capacitor
EIS	electrochemical impedance spectroscopy
F	Farads
F_c	Faraday's constant
g	gram
G	external circuit
i	current
i_d	current density
i_o	exchange current
k	kilo
K	Kelvin
l	electrode active layer thickness
l_s	separator thickness
L	inductor
LIB	lithium-ion battery
LIC	lithium-ion capacitor
m	milli
M	noles
n_e	number of electrons per ion
P	power
r	particle radius
R	resistor
R_u	universal gas constant
R_{ct}	charge transfer resistance
R_s	series resistance
R_W	Warburg impedance

Continued

SOC	state of charge
$T(P)$	temperature as a function of power
T_a	ambient temperature
T_{check}	temperature computed from C_W value
T_{check2}	temperature computed from C_{dl} value
T_{exp}	temperature computed from experimental energy results
T_{mod}	temperature computed from model's energy computations
$v(t)$	voltage as a function of time
V	voltage
$V_{dl//CT}$	voltage drop across double layer capacitance and charge transfer resistance
V_S	voltage drop across series resistance
V_W	voltage drop across Warburg elements
W	watt
W·h	watt-hour
α_a	anode specific surface area
α_c	cathode specific surface area
ΔV	change in voltage
ΔT	observed temperature change
δ	Nernst diffusion coefficient
ε	porosity
η	activation overpotential
μ	micro
ρ	density
Ω	Ohm